Front. Struct. Civ. Eng. 2022, 16(6): 718–728
https://doi.org/10.1007/s11709-022-0815-3

RESEARCH ARTICLE

Study of the mechanics of progressive collapse of FPB isolated beam-pier substructures

Jingcai ZHANG[a,b], Yong DING[a,b], Xinchun GUAN[a,b*]

[a] *Key Lab of Structures Dynamic Behavior and Control of the Ministry of Education, Harbin Institute of Technology, Harbin 150090, China*

[b] *Key Lab of Smart Prevention and Mitigation of Civil Engineering Disasters of the Ministry of Industry and Information, Harbin Institute of Technology, Harbin 150090, China*

[*] *Corresponding author. E-mail: guanxch@hit.edu.cn*

ABSTRACT The horizontal stiffness of the isolated layer is reduced substantially by a friction pendulum bearing (FPB) toprotectthe structure from potential damages caused by earthquakes. However, horizontal stiffness is essential to progressive collapse resistance of structures. This paper presents a simplified model to assess the progressive collapse response of beam-pier substructure isolated by FPB. Progressive collapse resistance by flexural action of the beam and additional resistance owing to the horizontal restraining force was achieved. The influences of the equivalent radius and friction coefficient of the FPB, the applied axial force on the FPB, and span-depth ratio of the beam on the additional resistance were investigated. Simulations were conducted to verify the proposed model. The results show that progressive collapse resistance provided by horizontal restraining can be reduced as large as 46% and 88% during compressive arching action (CAA) and catenary action (CA), respectively. The equivalent radius of the FPB shows limited effect on the progressive collapse response of FPB isolated structures, but friction coefficient and applied axial force, as well as depth ratio of the beam, show significant influences on the additional progressive collapse resistance capacity. Finite element method (FEM) results are in good agreement with the result obtained by the proposed method.

KEYWORDS friction pendulum bearing, progressive collapse, horizontal stiffness, compressive arching action, catenary action

1 Introduction

Progressive collapse is the spreading of an initial local failure from element to element, eventually resulting in the collapse of an entire structure or a large part of it. Almost all types of public and private buildings may be subjected to extreme events (i.e., hurricanes, tsunamis, earthquakes, explosions, vehicle impacts, fires and human errors, or even terrorist attacks). Such events usually cause local damage to the structure of buildings, but this can lead to a complete collapse. Furthermore, as it is difficult to predict the probability of occurrence and the magnitude of extreme events; it is neither practical nor possible to design a structure that is proof against such events through the traditional methods for conventional loads [1].

Over the past several decades, buildings around the world have suffered from partial or total progressive collapse, and many researchers focus their studies on the mechanics of structures; many measures have been proposed to prevent structures from progressive collapse. Theoretical analyses and experimental investigations as well as simulations, have been conducted to address progressive collapse mechanisms [1–5], typical static load-carrying mechanism curves and data have been obtained for both cast-in-place structure and prefabricated structure [6–10]. Structural performances have also been evaluated [11–14]. Furthermore, dynamic effects have also been assessed based on experimental and theoretical results [15–17]. It must be noted that most researchers

Article history: Received Jun 21, 2021; Accepted Dec 27, 2021

have focused their studies on traditional structures, i.e., fixed-base structures. Traditional structures usually have sufficient horizontal restraint conditions. Methods for improving progressive collapse resistance and existing design methods for progressive collapse both assume that sufficient horizontal restraint conditions can be provided by the beams and slabs [18,19].

However, it is believed that the horizontal restraint of a structure is vital for resisting progressive collapse [20]. Corley et al. [21] firstly declared that insufficient horizontal restraint could lead to more damage in progressive collapse accidents by investigating the collapse event of Alfred P. Murrah Federal Building in 1995. Experimental and simulation results from Diao show that insufficient horizontal restraint results in reducing the contribution of the axial force to the collapse resistance [22]. Both progressive collapse resistance and failure mode of frames were susceptible to boundary conditions [23–26]. Experimental results show that the vertical restraint is inextricably linked to the horizontal restraint of the structure, as reported in Ref. [23]. Also, the experimental and numerical results based on structures isolated by rubber bearings show that the catenary action (CA) cannot be formed due to weak horizontal constraint of the isolation layer [27–29].

Many methods and devices have been proposed to reduce structural vibration, such as the Tuned Mass Dampers [30–33], Pounding Tuned Mass Dampers [34], Tuned Liquid Dampers [35], MRE-Tuned Mass Dampers [36], Active Mass Dampers [37], and many other traditional dampers [38–48]. These traditional dampers show limited influences on the progressive collapse resistance of the structure. However, friction pendulum bearing (FPB) is an innovative technology for reducing vibration and protecting structures from damage due to earthquake; it mitigates the vibration of the isolated structure by extending the structure's fundamental period through reducing the horizontal stiffness of isolated layer [49]. This is quite different from the mechanisms of the aforementioned traditional dampers, which provide additional control force for suppressing structural vibration. Therefore, the horizontal stiffness of structure isolated by FPBs is much smaller than is the case for non-isolated structures controlled by traditional dampers. Moreover, the horizontal stiffness of the FPB is nonlinear, and it is influenced by the equivalent radius of axial force applied to the FPB, by the friction coefficient between the slider, and by the curved sliding surface as well as by the equivalent radius of the curved sliding surface. It means that the progressive collapse response of the structure with FPBs is essentially different from those of non-isolated structural systems and more complicated than those without any isolators. However, almost no papers focus on progressive collapse responses of structures equipped with FPBs.

This paper aims to investigate the progressive collapse resistance of pier-beam substructure from structure isolated by FPB and expand understandings of effects of the key factors of FPB isolated structures, including the equivalent radius, friction coefficient, axial force of FPB, and span-depth ratio of the beam, on the progressive collapse response of the pier-beam substructure. To this end, the primary substructure was considered as a simplified model based on the assumption that plane sections remain plane; the axial plastic strain responses of the beam were also ignored. Then, contributions to progressive collapse resistance provided by flexural action of the beam and horizontal restraining were assessed, respectively. Static analyses were performed to establish a theoretical static model for evaluating progressive collapse resistance of pier-beam substructure based on the simplified model. Finally, finite element method (FEM) simulations were conducted to verify the accuracy of the proposed model. The proposed model can be adopted to evaluate the progressive collapse resistance of a pier-beam substructure from structure isolated by FPB and can help to expand understanding of the effect of the key factors of the FPB isolated structure.

2 Overall progressive collapse resistance of FPB isolated substructure

The structural components that can provide resistance to the unbalanced gravity load are referred to as the 'substructure' [50]. The substructure is the smallest component of the entire structure that is intended to prevent progressive collapse.

An FPB isolated substructure for analysis in this paper is shown in Fig. 1, the progressive collapse resistance of the substructure (noted as P) can be given as Eq. (1).

$$P = P_{\mathrm{F}} + P_{\mathrm{H}}, \tag{1}$$

where P_{F} represents the contribution to progressive collapse resistance provided by flexural action of the beam, and P_{H} signifies the progressive collapse resistance provided by horizontal restraining.

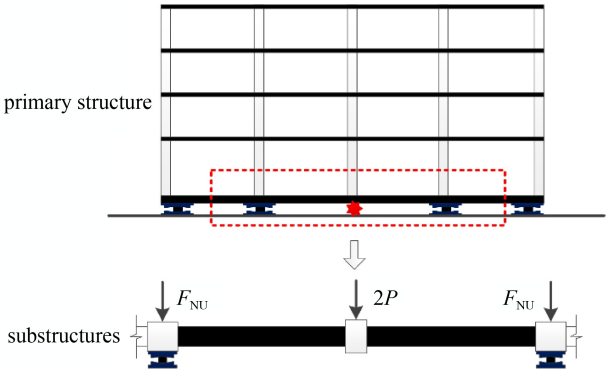

Fig. 1 Schematic of FPB isolated beam-pier substructure.

3 Assessment of progressive collapse resistance provided by horizontal restraining

The major difference between the FPB-isolated and non-isolated structures is that the FPB-isolated structures equipped with FPBs result in a significant reduction of horizontal restraint of the substructure, while the non-isolated structure possesses sufficient horizontal restraint conditions. In this section, progressive collapse resistance provided by horizontal restraining is discussed in detail.

3.1 Structural modeling

To investigate the progressive collapse resistance provided by horizontal restraint of the FPB isolated beam-pier substructures, i.e., R_H, the structural system displayed in Fig. 1 was simplified as shown in Fig. 2, and the following assumptions were made.

1) The FPB isolated beam-pier substructure was symmetrical about the missing column.

2) The beam section was considered rigid, and axial deformation was ignored.

3) The rotational degree of freedom of the structure was considered as hinged support, incapable of transmitting bending moments.

A nonlinear elastic spring was employed to simulate the direction behavior of the system.

The relationship between the beam vertical deflection (marked as δ_V) and the horizontal deformation (marked as δ_H) is given as Eq. (2),

$$\delta_H = -\frac{\delta_V(\delta_V - 2h_e)}{2L}, \tag{2}$$

where h_e is the effective depth of the beam which can be obtained by Eq. (3),

$$h_e = \frac{0.00473L^2}{H}. \tag{3}$$

Based on the energy conservation of the system,

$$F_H = k_{FPB}\delta_H. \tag{4}$$

Therefore, P_H can be given as Eq. (5),

$$P_H = k_{FPB}\frac{\delta_V(2h_e - \delta_V)(h_e - \delta_V)}{2L^2}. \tag{5}$$

3.2 Horizontal restraint provided by FPB

Since FPB was invented by Zayas et al. [49], various types of FPB have been proposed. One of the most extensively used FPB is shown in Fig. 3, and it consists of three parts: two curved sliding surfaces and a slider embedded coated in PTFE. The friction coefficient between the slider and curved sliding surfaces is quite low to prevent earthquake energy transmitting to superstructures.

Based on the location of the slider on the sliding surface, the horizontal stiffness of FPB can be divided into two main stages. When $d \leqslant d_y$, no sliding occurs between the slider and curved sliding surface just as shown in Fig. 3(a); the horizontal stiffness is presented as k_p as exhibited in Fig. 3(c). At this stage, the horizontal restraint provided by FPB can be simulated as a linear spring. Otherwise, the horizontal stiffness is k_e as shown in Fig. 3(c), and a nonlinear elastic spring can be employed to simulate the horizontal restraint of the system. Consequently, the horizontal stiffness of the isolators can be expressed as Eq. (6).

$$k_{FPB} = \begin{cases} \dfrac{\mu F_{NU}}{d_y}, & d \leqslant d_y, \\ \dfrac{\left(\mu + \operatorname{sig}(\dot{d}) \cdot \dfrac{d}{R_E}\right)F_{NU}}{d}, & d > d_y, \end{cases} \tag{6}$$

where F_{NU} is the axial force applied on FPB, μ is the friction coefficient between the slider and curved sliding surface, d_y is the yield displacement of FPB, d is the sliding displacement of FPB, R_E is the equivalent radius of FPB which can be obtained by Eq. (7):

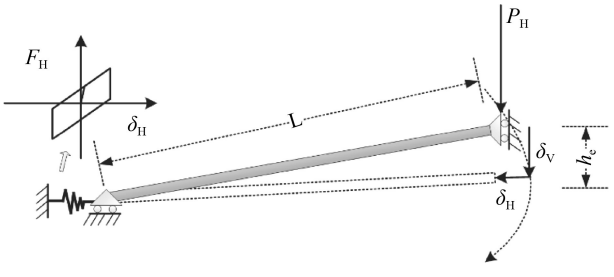

Fig. 2 Structural representation for modeling.

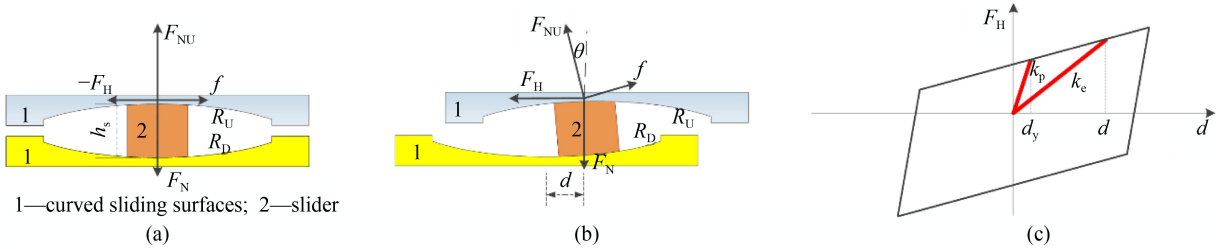

Fig. 3 Mechanic schematic of FPB. (a) Without sliding stage; (b) sliding stage; (c) horizontal constraint.

$$R_{\mathrm{E}} = R_{\mathrm{U}} + R_{\mathrm{D}} - h_{\mathrm{s}}, \tag{7}$$

where R_{U} and R_{D} are the curvature radius of the curved sliding surface, respectively. h_{s} is the height of the slider.

3.3 Compressive arching action

According to Eq. (5), P achieves the maximum when $\delta_{\mathrm{V}} = 0.423h_{\mathrm{e}}$. However, δ_{H} and F_{H} achieve their maximum, $\delta_{\mathrm{H0}} = 0.5(h_{\mathrm{e}})^2/L$ and $F_{\mathrm{H0}} = 0.5k_{\mathrm{FPB}}\ (h_{\mathrm{e}})^2/L$, when $\delta_{\mathrm{V}} = h_{\mathrm{e}}$, respectively. Therefore, the relationship between δ_{H0} and d_{y} can be adopted to determine whether sliding occurs or not, and sliding occurs when $\delta_{\mathrm{H0}}/d_{\mathrm{y}}$ is larger than 1 (Eq. (8)).

$$\frac{\delta_{\mathrm{H0}}}{d_{\mathrm{y}}} \geqslant 1. \tag{8}$$

By substituting Eq. (3) into Eq. (8), it can be seen that the geometrical parameters of the beam (i.e., H and L) are the factors that decide whether the FPB slider is sliding or not.

Influences of L/H and L on the δ_{H0}/d are shown in Fig. 4. When $\delta_{\mathrm{H0}} = d_{\mathrm{y}}$ (the red solid line in Fig. 4), the sliding occurs. The results show that $\delta_{\mathrm{H0}}/d_{\mathrm{y}}$ increases with L increasing, and larger $\delta_{\mathrm{H0}}/d_{\mathrm{y}}$ will be obtained. Moreover, $\delta_{\mathrm{H0}}/d_{\mathrm{y}}$ is proportional to L/H. The minimum L when sliding occurs is 0.9 m. But for almost all of the beams in engineering, L is longer than 0.9 m, which means that sliding occurs in almost all situations.

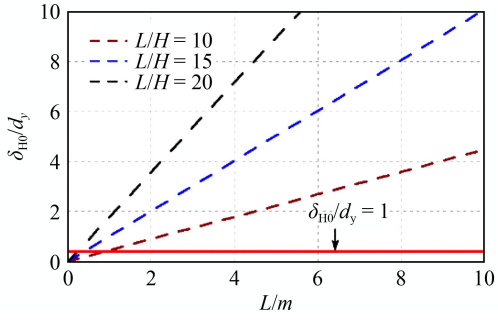

Fig. 4 Influence of L/H and L on the δ_{H0}/d.

Therefore, the δ_{V1} and δ_{V2} corresponding to vertical deflection when sliding occurs can be expressed as

$$\delta_{\mathrm{V1}} = h_{\mathrm{e}} - \sqrt{h_{\mathrm{e}}^2 - 2Ld_{\mathrm{y}}}, \tag{9a}$$

$$\delta_{\mathrm{V2}} = h_{\mathrm{e}} + \sqrt{h_{\mathrm{e}}^2 - 2Ld_{\mathrm{y}}}. \tag{9b}$$

It's obvious that δ_{V1} and δ_{V2} only depend on the geometrical parameters, and they are independent of the properties of the FPB isolators, i.e., R_{E} and μ. The horizontal reaction force and the resisting capacity, F_{H} and P_{H}, respectively, can be given as Eqs. (10) and (11):

$$F_{\mathrm{H}} = \begin{cases} \dfrac{\mu F_{\mathrm{NU}}\delta_{\mathrm{V}}(2h_{\mathrm{e}} - \delta_{\mathrm{V}})}{2Ld_{\mathrm{y}}}, \\ \quad 0 < \delta_{\mathrm{V}} \leqslant \delta_{\mathrm{V1}} \text{ or } h_{\mathrm{e}} < \delta_{\mathrm{V}} \leqslant \delta_{\mathrm{V2}}, \\ \dfrac{F_{\mathrm{NU}}\left[\delta_{\mathrm{V}}(2h_{\mathrm{e}} - \delta_{\mathrm{V}}) + 2\mathrm{sig}\left(\dot{\delta}_{\mathrm{H}}\right)LR_{\mathrm{E}}\mu\right]}{2LR_{\mathrm{E}}}, \\ \quad \delta_{\mathrm{V1}} < \delta_{\mathrm{V}} \leqslant h_{\mathrm{e}} \text{ or } \delta_{\mathrm{V2}} < \delta_{\mathrm{V}} \leqslant 2h_{\mathrm{e}}, \end{cases} \tag{10}$$

$$P_{\mathrm{H}} = \begin{cases} \dfrac{\mu F_{\mathrm{NU}}\delta_{\mathrm{V}}(h_{\mathrm{e}} - \delta_{\mathrm{V}})(2h_{\mathrm{e}} - \delta_{\mathrm{V}})}{2L^2d_{\mathrm{y}}}, \\ \quad 0 < \delta_{\mathrm{V}} \leqslant \delta_{\mathrm{V1}} \text{ or } h_{\mathrm{e}} < \delta_{\mathrm{V}} \leqslant \delta_{\mathrm{V2}}, \\ \dfrac{F_{\mathrm{NU}}(h_{\mathrm{e}} - \delta_{\mathrm{V}})\left[\delta_{\mathrm{V}}(2h_{\mathrm{e}} - \delta_{\mathrm{V}}) + 2\mathrm{sig}\left(\dot{\delta}_{\mathrm{H}}\right)LR_{\mathrm{E}}\mu\right]}{2L^2R_{\mathrm{E}}}, \\ \quad \delta_{\mathrm{V1}} < \delta_{\mathrm{V}} \leqslant h_{\mathrm{e}} \text{ or } \delta_{\mathrm{V2}} < \delta_{\mathrm{V}} \leqslant 2h_{\mathrm{e}}. \end{cases} \tag{11}$$

3.4 Catenary action

When $P = 0$ and $\delta_{\mathrm{V}} = 2h_{\mathrm{e}}$, the slider slides back to the center of the surface. Then tensile CA starts to work. The derivation of horizontal reaction force and resisting capacity of the substructure in the CA stage is similar to derivation in the compressive arching action (CAA) stage, the corresponding vertical deflection, defined as δ_{V3}, can be obtained as Eq. (12),

$$\delta_{\mathrm{V3}} = h_{\mathrm{e}} + \sqrt{h_{\mathrm{e}}^2 + 2Ld_{\mathrm{y}}}. \tag{12}$$

And F_{H} and P_{H} can be given as Eqs. (13) and (14), respectively.

$$F_{\mathrm{H}} = \begin{cases} \dfrac{\mu F_{\mathrm{NU}}\delta_{\mathrm{V}}(2h_{\mathrm{e}} - \delta_{\mathrm{V}})}{2Ld_{\mathrm{y}}}, & 2h_{\mathrm{e}} < \delta_{\mathrm{V}} \leqslant \delta_{\mathrm{V3}}, \\ \dfrac{F_{\mathrm{NU}}\left[\delta_{\mathrm{V}}(2h_{\mathrm{e}} - \delta_{\mathrm{V}}) + 2\mu\mathrm{sig}\left(\dot{\delta}_{\mathrm{H}}\right)LR_{\mathrm{E}}\right]}{2LR_{\mathrm{E}}}, & \delta_{\mathrm{V}} > \delta_{\mathrm{V3}}, \end{cases} \tag{13}$$

$$P_{\mathrm{H}} = \begin{cases} \dfrac{\mu F_{\mathrm{NU}}\delta_{\mathrm{V}}(h_{\mathrm{e}} - \delta_{\mathrm{V}})(2h_{\mathrm{e}} - \delta_{\mathrm{V}})}{2L^2d_{\mathrm{y}}}, & 2h_{\mathrm{e}} < \delta_{\mathrm{V}} \leqslant \delta_{\mathrm{V3}}, \\ \dfrac{F_{\mathrm{NU}}(h_{\mathrm{e}} - \delta_{\mathrm{V}})\left[\delta_{\mathrm{V}}(2h_{\mathrm{e}} - \delta_{\mathrm{V}}) + 2\mu\mathrm{sig}\left(\dot{\delta}_{\mathrm{H}}\right)LR_{\mathrm{E}}\right]}{2L^2R_{\mathrm{E}}}, & \delta_{\mathrm{V}} > \delta_{\mathrm{V3}}. \end{cases} \tag{14}$$

3.5 Evaluation and comparison

To evaluate the structure's complete analytical horizontal and vertical restraining response, the dimensionless method is applied to the analysis. The dimensionless force $F_{\mathrm{H}}/F_{\mathrm{H0}}$ and P/P_{CAA0} were used to measure the horizontal and vertical restraints, where F_{H0} and P_{CAA0} are the corresponding maxima of the structure without sliding (see Eqs. (15) and (16)).

$$P_{CAA0} = k_p \frac{0.193 h_e^3}{L^2}, \tag{15}$$

$$F_{H0} = k_p \frac{h_e^2}{2L}. \tag{16}$$

The full range of the behavior that includes the compressive arching action and the tensile catenary action is presented in Fig. 5. OABD represents CAA, and DF is characteristic of CA.

Before Point A, the horizontal stiffness of the structure is k_p which is a constant. It is observed that F_H/F_{H0} increases proportionally with the increase of δ_V. As a result, P/P_{CAA0} increases with the increase of δ_V. Regarding Point A, sliding occurs, the horizontal stiffness shifted from k_p to k_e, and k_e decreases with the increase of δ_V, leading to slight increases in F_H/F_{H0}. Moreover, sliding results in a decrease of P/P_{CAA0}. Finally, δ_H reaches the maximum, and F_H exhibits a snap-through instability until a new position of stable equilibrium is adopted from Point A to Point B because frictional force starts decreasing, P falls to zero at Point B ($\delta_V = h_e$).

It should be noted that F_H increases from Point B ($\delta_V = h_e$) to Point D ($\delta_V = 2h_e$) which differs from the results for the non-isolated structure.

After the slider has gone back to the bottom of the curved sliding surface at Point D, it is the end of the CAA and the start of the CA. The contribution by catenary action increases gradually with increasing deflection.

3.6 Parametric analysis

The essential distinction between a structure with FPB and a non-isolated structure is the significant reduction of horizontal stiffness due to the FPB. In other words, the main differences between the two types of structure are the additional resistance owing to the horizontal restraining force, i.e., F_H (see Eq. (6)).

In this section, parameter studies were conducted to have precise and deep insight into the influence factors on P. The model is from the structure designed by Lu et al. [8]; FPB isolated pier-column substructures were fabricated by using FPBs on the top of the frame bottom column as shown in Fig. 1.

3.6.1 Comparison between FPB-isolated and non-isolated substructures

Comparisons between FPB-isolated and non-isolated structures are shown in Fig. 6. Both horizontal and vertical restraints of FPB isolated structures are much less than the case for the fixed-base structures. The maximum F_H in the CAA stage, for FPB-isolated and fixed-base structures are $0.28F_{H0}$ and $1.19F_{H0}$, respectively. Only 23% horizontal restraining can be offered by FPB-isolated compared to that of the fixed-base structure. Moreover, when $\delta_V = 4h_e$, F_H of the FPB-isolated structure is $0.53F_{H0}$, the corresponding value was $4.39F_{H0}$ for the fixed-base structure. The reduction of F_H leads to

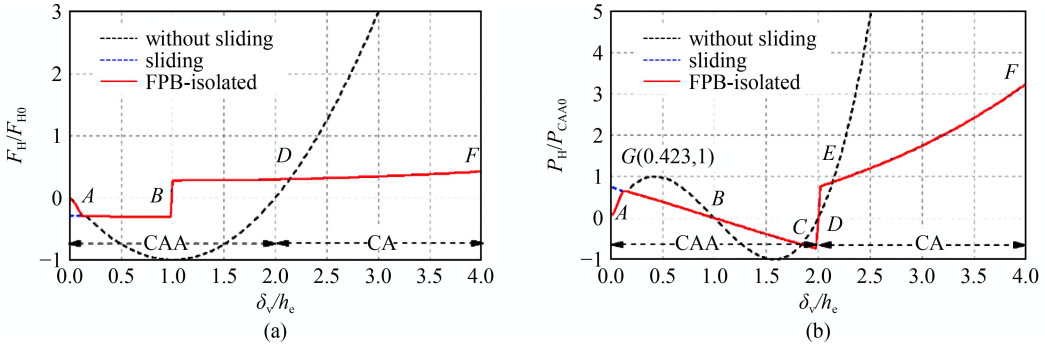

Fig. 5 Complete analytical additional resistance response of the structure. (a) Horizontal restraint; (b) vertical restraint.

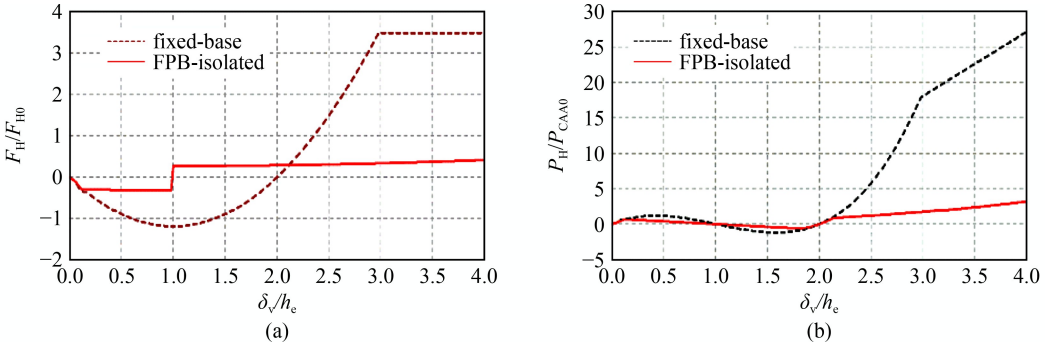

Fig. 6 Comparison between FPB-isolated and non-isolated structure. (a) Horizontal restraint; (b) vertical restraint.

a significant decrease in P. The maximum P is 1.19 P_{CAA0} for fixed-base structure, but only $0.64P_{CAA0}$ for isolated structure. Furthermore, P is $3.23P_{CAA0}$ and $27.2P_{CAA0}$ for FPB-isolated and fixed-base structure respectively when $\delta_V = 4h_e$.

The results indicate that the capacity of resisting progressive collapse of structure is significantly compromised by FPB isolators considering that the progressive collapse resistance provided by horizontal restraining, i.e., P_H, can be 30% of the P for fixed-base structure in CAA and an ever-larger proportion in CA.

3.6.2 Equivalent radius

Figure 7 displays the influence of equivalent radius, i.e., R_E, on the horizontal restraining and vertical restraining of the substructure isolated by FPB when μ is 0.05. It's obvious that R_E has almost no effect on horizontal restraining and vertical restraining. R_E affected only the horizontal stiffness of the isolator when sliding occurs based on Eq. (6). Therefore, all cases show the same result before sliding. After sliding in CAA, R_E has not shown remarkable impacts on k_{FPB} since the δ_H is small, and P_H is still a small fraction of the total horizontal restraining (Eq. (6)). It is dominated by the friction force between sliding and curved sliding surfaces. For instance, P is $0.392P_{CAA0}$, $0.384P_{CAA0}$, $0.380P_{CAA0}$, and $0.378P_{CAA0}$ responding to R_E are equal to 1, 2, 3, and 4 m, respectively. The result differences are no more than 5 percent in all cases.

However, the effect of R_E becomes more and more obvious with the development of deflection. For example, P is $2.76P_{CAA0}$, $2.60P_{CAA0}$, and $2.52P_{CAA0}$ when R_E is 2, 3, and 4 m, respectively.

In summary, R_E showed limited effect on the progressive collapse response of FPB isolated pier-column substructures, especially when δ_H was small.

3.6.3 Friction coefficient

The influence of friction coefficient on horizontal and vertical restraining is displayed in Fig. 8. Significant differences both in F_H/F_{H0} and P_H/P_{CAA0} can be found when the friction coefficient of the isolator (noted as μ) ranges from 0.025 to 0.10 because k_{FPB} can be improved by increasing friction coefficient μ. When μ is equal to 0.025 and 0.05, the most used in many areas of civil engineering, the maxima of P in CAA are only $0.31P_{CAA0}$ and $0.61P_{CAA0}$, respectively. The corresponding values can be increased to $0.91P_{CAA0}$ and $1.22P_{CAA0}$ when μ is increased to 0.075 or ever 0.10. Meanwhile, F_H/F_{H0} and P/P_{CAA0} can be improved significantly utilizing a higher friction coefficient of FPB.

It should be noted that higher friction coefficient means more earthquake energy will be transmitted from the ground to the superstructure, and severe vibration will be suffered. Therefore, both vibration reduction and progressive collapse restraining should be comprehensively considered in choosing the friction coefficient of FPB.

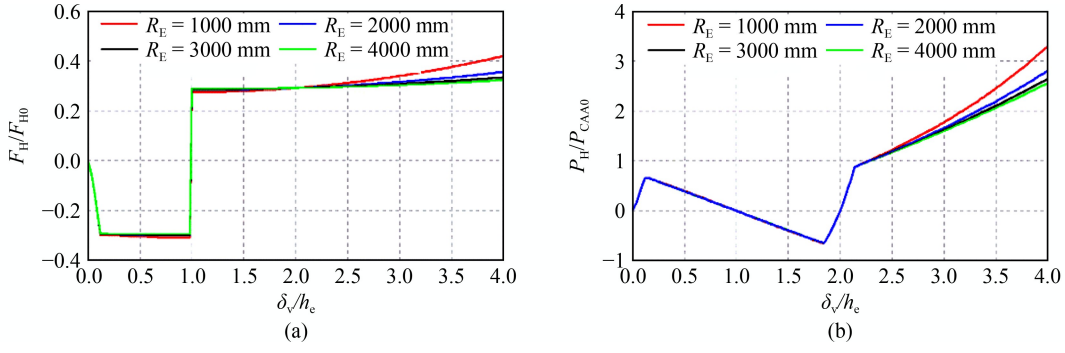

Fig. 7 Influence of equivalent radius on (a) horizontal restraining and (b) vertical restraining.

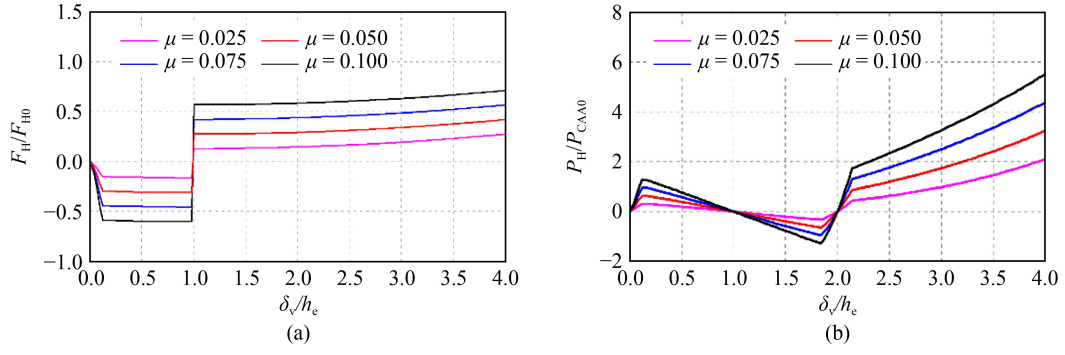

Fig. 8 Influence of friction coefficient on (a) horizontal restraining and (b) vertical restraining.

3.6.4 Axial force applied on FPB

It is evidence that both F_H/F_{H0} and P_H/P_{CAA0} can be improved effectively through higher axial force applied on FPB (Fig. 9). It also shows that horizontal stiffness of FPB can be enhanced by higher axial force whether or not sliding occurs.

3.6.5 Depth ratio of the beam

The influence of the depth ratio of the beam on the horizontal and vertical restraining can be found in Fig. 10. It can be concluded that a higher h_e can be obtained by increasing the depth ratio of the beam. Therefore, superior vertical restraining can be achieved notwithstanding the almost same horizontal restraining in CAA. In a later period of CA, horizontal restraining increased obviously, leading to markedly improved vertical restraining. For instance, when $\delta_V = 4h_e$, F_H is $0.42F_{H0}$ and $0.47F_{H0}$ corresponding to $L/H = 10$ and 12, about 20% improvement comparing to $L/H = 8$. More remarkable improvement can be obtained for P_H, P_H is $3.23P_{CAA0}$ and $4.19P_{CAA0}$, when L/H is equal to 8 and 10, respectively, with 46% and 90% increase comparing to $L/H = 8$.

4 Assessment of progressive collapse resistance by flexural action

The contribution of flexural action to progressive collapse resistance of the beam-pier substructure can be simplified as a polygonal line model as shown in Fig. 11. Point Y represents the case of a beam section at the first yield of longitudinal reinforcement. Point P represents the case of substructure at the maximum bearing capacity of the beam mechanism stage, and Point U represents the bearing capacity provided by the steel.

At Point Y of the polygonal line model [51,52],

$$P_F^y = \frac{4M_y}{L}, \tag{17}$$

$$\delta_v^y = \frac{\varphi_1 l_1}{2}\left(L - \frac{l_1}{3}\right) + \frac{\varphi_y l_2^2}{6}. \tag{18}$$

where M_y is the moment on both sides of the middle column at first yield.

At Point P,

$$P_F^p = \frac{2(M_{P1} + M_{P2})}{L}, \tag{19}$$

$$\delta_v^p = \frac{\varphi_{y1} l_1}{2}\left[L - \frac{l_1}{3}\right] + \frac{\varphi_{y2} l_2^2}{6} + [\varphi_{p1} - \varphi_{y1}] l_{11}\left[L_1 - \frac{l_{11}}{2}\right] + \frac{(\varphi_{p2} - \varphi_{y2}) l_{12}^2}{2}, \tag{20}$$

$$M_{P1} = f_y A'_{s1}(H - a'_s) + \alpha_1 f_c b x\left(h_0 - \frac{x}{2}\right), \tag{21}$$

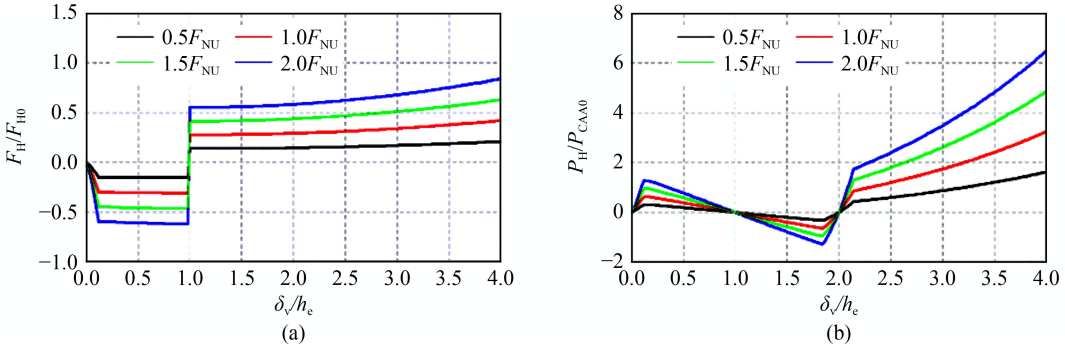

Fig. 9 Influence of axial force on (a) horizontal restraining and (b) vertical restraining.

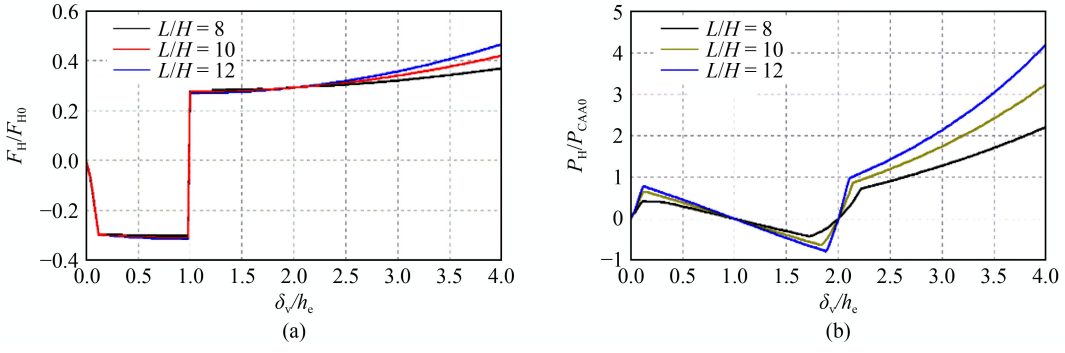

Fig. 10 Influence of the depth ratio of the beam on (a) horizontal restraining and (b) vertical restraining.

$$M_{P2} = M_{U2} = f_y A'_{s2}(H - 2a_s), \tag{22}$$

where M_y is the moment on both sides of the middle column at first yield, φ_y represents the curvature of sections of the beam end sections at first yield moment, φ_p the curvature of the beam end sections at maximum moment.

Regarding Point U, concrete of the beam end sections has been crushed, and P_v^u can be given as

$$P_F^u = \frac{2(M_{U1} + M_{U2})}{L}, \tag{23}$$

$$M_{U1} = f_y A'_{s1}(H - 2a_s), \tag{24}$$

$$M_{U2} = M_{P2}, \tag{25}$$

$$\delta_v^u = 10\delta_v^y. \tag{26}$$

Therefore, the complete analytical representation of the FPB isolated pier-column substructures can be obtained and is shown in Fig. 12.

5 Verification of the proposed model

Since no collapse experiments on the FPB isolated structure have been conducted, FEM simulations were conducted to verify the accuracy of the proposed model. FEM studies on a one-storey substructure (shown as Fig. 13(a)) in ABAQUS software, and the equivalent radius (R_E) and the friction coefficient (μ) of the FPB were 1 m and 0.05; the axial force applied on the column was 100.4 kN.

The FEM model is shown in Fig. 13(b). The concrete was all modeled as a C3D8R solid element as an 8-node linear brick, with reduced integration and hourglass control element. The rebar was modeled using T3D2 element. The mesh size was set as 20 mm for concrete and rebar.

Comparison between the proposed model results and FEM results is shown in Fig. 14 and Table 1. Obvious characteristics of CAA and CA can be found. But there are still gaps between the FEM results and the proposed method results. On the one hand, the axial deformations were ignored in the proposed idea, but there are still deformations in the axial direction of the beam bridging the failed column in FEM. On the other hand, beam sections were considered rigid, but plastic deformation of concrete on the end of the beam will also dissipate part of energy in FEM. However, the maximum error of the four key parameters between the proposed model and FEM results did not exceed 8%. Consequently, the proposed method is capable of predicting behavior of FPB isolated beam-pier substructures during progressive collapse.

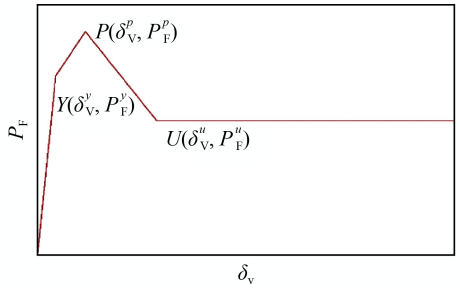

Fig. 11 The simplified model for flexural action of the column-beam structure.

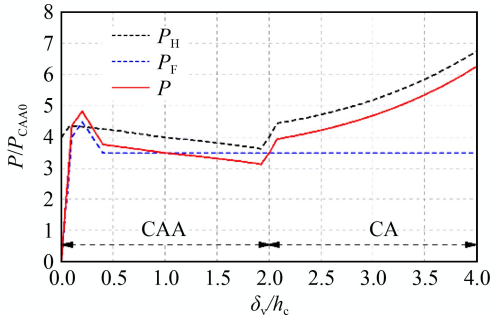

Fig. 12 Complete analytical representation of the FPB isolated pier-column substructures.

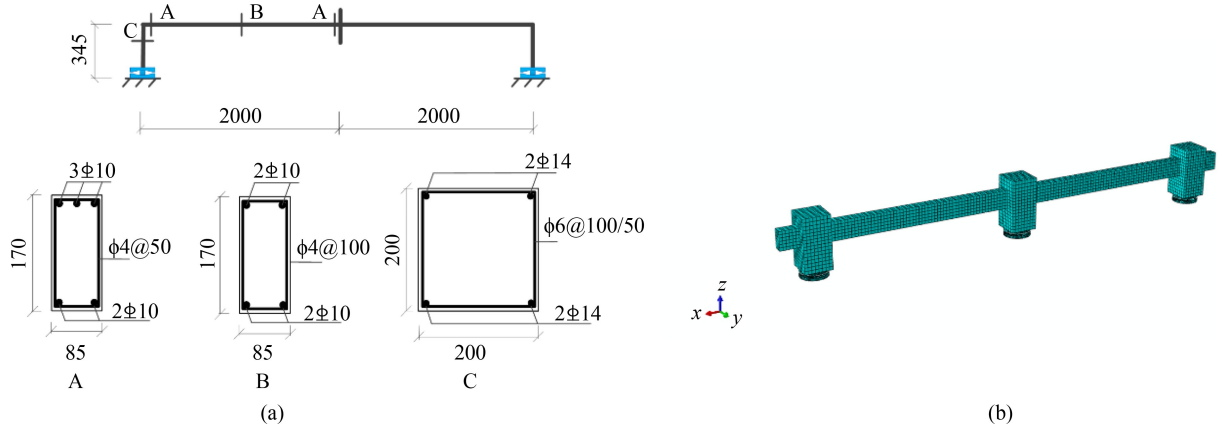

Fig. 13 Details of the one-storey substructure and FEM model. (a) Details of the substructures; (b) model in Abaque software.

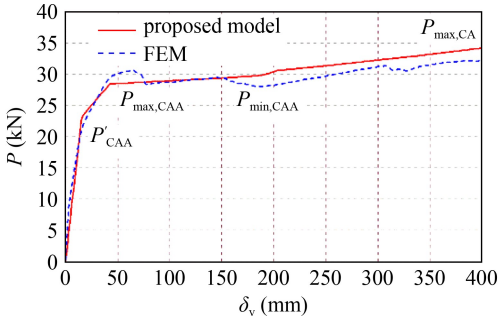

Fig. 14 Comparison of the FEM results and the proposed method results.

Table 1 Comparison of the FEM results and the proposed method results

parameter	FEM (kN)	proposed model (kN)	$\frac{\lvert\text{FEM} - \text{proposed model}\rvert}{\text{FEM}}$
P'_{CAA}	21.0	22.5	7.14%
$P_{max,CAA}$	30.7	28.5	7.16%
$P_{min,CAA}$	28.1	29.4	2.49%
$P_{max,CA}$	32.2	34.2	6.21%

6 Discussion

The overall progressive collapse resistance of FPB isolated substructure can be easily obtained based on Eqs. (1), (5), and (17)–(26). Researchers and engineers can also adjust the parameters of the superstructure and FPBs based on the result to satisfy the requirements of different FPB isolated buildings.

The substructure was simplified for analysis; the beam section was considered rigid and axial deformation was ignored, therefore error may be caused. This is the main reason for the gap between the proposed model result and FEM result presented in Section 5. However, the proposed model can be adopted to evaluate the progressive collapse resistance of pier-beam substructure from structure isolated by FPB and help to expand understandings of the effects of the key factors of the FPB isolated structure, since the gap between the FEM results and the proposed method results are insignificant. Therefore, the proposed methodology can be used for most buildings. However, assessment of progressive collapse resistance provided by horizontal restraining is based on the assumption that the structure is symmetrical about the missing column. For an unsymmetrical structure, such as when the corner column is damaged, the resistance would be overestimated and this needs further research. Moreover, experiments should be conducted to give insight into the mechanics of progressive collapse of FPB isolated structures and the proposed method's accuracy when applied to practical engineering.

The depth of beams above the FPB isolators is usually much larger than that of the beams in a typical story. Therefore, the contribution to progressive collapse resistance provided by flexural action of the beam can be enhanced compared with the substructure in a typical story, and enhancements by the larger depth of beams need to be further investigated. Furthermore, corresponding ultimate deformations for compressive arching action and catenary actions are usually set to be $0.06L$ and $0.2L$ (where L is the span of the beam) for progressive collapse investigations, respectively. The heights of the isolation layer are larger than $0.06L$ and $0.2L$ for most isolated buildings. For those buildings with not enough room for beams to develop large deformation, i.e., space to accommodate the FPB isolators is shorter than $0.2L$, the isolator and piers would impact slab, and there will be more serious damage. Therefore, further studies are needed.

7 Conclusions

This paper presents a simplified model for static analysis of progressive collapse response of RC beam-pier substructures. The influences of the equivalent radius, friction coefficient, axial force of FPB, and span-depth ratio of the beam on the additional resistance were also investigated. Finally, simulations were conducted to verify the accuracy of the proposed model. The following conclusions can be drawn from the present study.

1) The progressive collapse resistance provided by horizontal restraining are reduced by FPB isolators significantly. And the progressive collapse resistance capacity of FPB isolated beam-column substructures was far less than those bare structures without FPB isolators.

2) The equivalent radius of FPB has almost no effect on the progressive collapse response of FPB isolated pier-column substructures, especially when the horizontal deformation of the beam is small in compressive arching action; it affects only the horizontal stiffness of the isolator when sliding occurs. But the effect of equivalent radius of FPB becomes more and more obvious with the development of the deflection in catenary action. The higher friction coefficient and larger axial force applied on FPB result in improvement of progressive collapse resistance, and superior vertical restraining can be achieved by increasing the depth ratio of the beam.

3) The accuracy of the proposed method was verified by FEM simulation, and the proposed approach is a simple but efficient method for addressing the mechanics of progressive collapse of FPB isolated beam-pier substructures in practical engineering.

Acknowledgements This research was supported by the National Key Research and Development Program of China (No. 2017YFC0703603).

References

1. Adam J M, Parisi F, Sagasetac J, Lu X Z. Research and practice on progressive collapse and robustness of building structures in the 21st century. Engineering Structures, 2018, 173: 122−149
2. Stylianidis P M, Nethercot D A, Izzuddin B A, Elghazouli A Y. Study of the mechanics of progressive collapse with simplified beam models. Engineering Structures, 2016, 117: 287−304
3. Lu X Z, Lin K Q, Li C, Li Y. New analytical calculation models for compressive arch action in reinforced concrete structures. Engineering Structures, 2018, 168: 721−735
4. Qian K, Li B, Ma J. Load-carrying mechanism to resist progressive collapse of RC buildings. Journal of Structural Engineering, 2015, 141(2): 04014107
5. Qian K, Li B. Strengthening and retrofitting precast concrete buildings to mitigate progressive collapse using externally bonded GFRP strips. Journal of Composites for Construction, 2019, 23(3): 04019018
6. Li Y, Lu X Z, Guan H, Ye L P. Progressive collapse resistance demand of reinforced concrete frames under catenary mechanism. ACI Structural Journal, 2014, 111(5): 1225−1234
7. Qian K, Weng Y H, Li B. Improving behavior of reinforced concrete frames to resist progressive collapse through steel bracings. Journal of Structural Engineering, 2019, 145(2): 04018248
8. Lu X Z, Lin K Q, Li Y, Guan H, Ren P, Zhou Y. Experimental investigation of RC beam-slab substructures against progressive collapse subject to an edge-column-removal scenario. Engineering Structures, 2017, 149: 91−103
9. Lu X, Lu X, Guan H, Ye L. Collapse simulation of reinforced concrete high-rise building induced by extreme earthquakes. Earthquake Engineering & Structural Dynamics, 2013, 42(5): 705−723
10. Qian K, Li B. Analytical evaluation of the vulnerability of RC frames for progressive collapse caused by the loss of a corner column. Journal of Performance of Constructed Facilities, 2015, 29(1): 04014025
11. Xiao Y, Kunnath S, Li F W, Zhao Y B, Lew H S, Bao Y. Collapse test of three-story half-scale reinforced concrete frame building. ACI Structural Journal, 2015, 112(4): 429−438
12. Marjanishvili S, Agnew E. Comparison of various procedures for progressive collapse analysis. Journal of Performance of Constructed Facilities, 2006, 20(4): 365−374
13. Mehrdad S, Marlon B, Serkan S. Experimental and analytical progressive collapse evaluation of actual reinforced concrete structure. ACI Structural Journal, 2007, 104(6): 731−739
14. Setareh H S, Mashhadi J. Assessment of dynamic increase factor for progressive collapse analysis of RC structures. Engineering Failure Analysis, 2017, 84: 300−310
15. Liu M. A new dynamic increase factor for nonlinear static alternate path analysis of building frames against progressive collapse. Engineering Structures, 2013, 48: 666−673
16. Tsai M H, Lin B H. Dynamic amplification factor for progressive collapse resistance analysis of an RC building. Structural Design of Tall and Special Buildings, 2009, 18(5): 539−557
17. Li Y, Lu X Z, Guan H, Ye L P. An improved tie force method for progressive collapse resistance design of reinforced concrete frame structures. Engineering Structures, 2011, 33(10): 2931−2942
18. UFC-4-023-03. Design of Structures to Resist Progressive Collapse. Washington D.C.: Department of Defense (DoD), 2009
19. General Service Administration (GSA). Progressive Collapse Analysis and Design Guidelines for New Federal Office Buildings and Major Modernization Projects. Washington D.C.: The US General Service Administration, 2003
20. Tan Z, Zhong W, Meng B, Zheng Y, Duan S. Effect of various boundary constraints on the collapse behavior of multi-story composite frames. Journal of Building Engineering, 2022, 52: 104412
21. Corley W G, Sozen M A, Thornton C H, Mlakar P F. The Oklahoma City Bombing: Improving Building Performance Through Multi-hazard Mitigation. Washington, D.C.: Federal Emergency Management Agency, 1996
22. Diao M Z, Li Y, Guan H, Lu X Z, Gilbert B P. Influence of horizontal restraints on the behavior of vertical disproportionate collapse of RC moment frames. Engineering Failure Analysis, 2020, 109: 104324
23. Kang S B, Tan K H, Liu H Y, Zhou X H, Yang B. Effect of boundary conditions on the behaviour of composite frames against progressive collapse. Journal of Constructional Steel Research, 2017, 138: 150−167
24. Lim N S, Tan K H, Lee C K. Effects of rotational capacity and horizontal restraint on development of catenary action in 2-d RC frames. Engineering Structures, 2017, 153: 613−627
25. Pham A T, Lim N S, Tan K H. Investigations of tensile membrane action in beam-slab systems under progressive collapse subject to different loading configurations and boundary conditions. Engineering Structures, 2017, 150: 520−536
26. Zhong W, Meng B, Hao J. Performance of different stiffness connections against progressive collapse. Journal of Constructional Steel Research, 2017, 135: 162−175
27. Du Y, Zhu X, Lu X Z, Song X, Tan Z. Analysis on progressive collapse resistance of long complicated isolated structures. China Civil Engineering Journal, 2012, S1: 90−95 (in Chinese)
28. Du Y, Shi C. Progressive collapse performance of isolated structures subjected to multi-direction coupled dynamic excitation. Engineering Mechanics, 2019, 36(6): 248−256
29. Du Y, Duan H, Xu T. Vertical progressive collapse mechanism and influencing factors of base-isolated structures. Journal of Vibration and Shock, 2018, 37(5): 257−260
30. Khatibinia M, Gholami H, Kamgar R. Optimal design of tuned mass dampers subjected to continuous stationary critical excitation. International Journal of Dynamics and Control, 2018, 6(3): 1094−1104
31. Kamgar R, Samea P, Khatibinia M. Optimizing parameters of tuned mass damper subjected to critical earthquake. Structural Design of Tall and Special Buildings, 2018, 27(7): e1460
32. Kamgar R, Khatibinia M, Khatibinia M. Optimization criteria for design of tuned mass dampers including soil–structure interaction effect. International Journal of Optimization in Civil Engineering, 2019, 9(2): 213−232
33. Dadkhah M, Kamgar R, Heidarzadeh H, Jakubczyk-Gałczyńska A,

Jankowski R. Improvement of performance level of steel moment-resisting frames using tuned mass damper system. Applied Sciences (Basel, Switzerland), 2020, 10(10): 3403

34. Xue Q, Zhang J, He J, Zhang C, Zhou G. Seismic control performance for pounding tuned massed damper based on viscoelastic pounding force analytical method. Journal of Sound and Vibration, 2017, 411: 362−377
35. Kamgar R, Gholami F, Zarif Sanayei H R, Heidarzadeh H. Modified tuned liquid dampers for seismic protection of buildings considering soil–structure interaction effects. Civil Engineering (Shiraz), 2020, 44(1): 339−354
36. Guan X, Zhang J, Li H, Ou J O U J. Semi-active control for benchmark building using innovative TMD with MRE isolators. International Journal of Structural Stability and Dynamics, 2020, 20(6): 2040009
37. Fitzgerald F, Sarkar S, Staino A. Improved reliability of wind turbine towers with active tuned mass dampers (ATMDs). Journal of Sound and Vibration, 2018, 419: 103−122
38. Shariati A, Kamgar R, Rahgozar R. Optimum layout of nonlinear fluid viscous damper for improvement the responses of tall buildings. International Journal of Optimization In Civil Engineering, 2020, 10(3): 411−431
39. Salimi M, Kamgar R, Heidarzadeh H. An evaluation of the advantages of friction TMD over conventional TMD. Innovative Infrastructure Solutions, 2021, 6(2): 1−12
40. Kamgar R, Heidarzadeh H, Samani M. Evaluation of buckling load and dynamic performance of steel shear wall retrofitted with strips made of shape memory alloy. Scientia Iranica, 2020, 1(1): 1−27
41. Kamgar R, Dolatabad Y A, Samani M R. Seismic optimization of steel shear wall using shape memory alloy. Iran University of Science & Technology, 2019, 9(4): 671−687
42. Dadkhah M, Kamgar R, Heidarzadeh H. Improving the nonlinear seismic performance of steel moment-resisting frames with minimizing the ductility damage index. SN Applied Sciences, 2021, 3(1): 1−14
43. Tavakoli R, Kamgar R, Rahgozar R. Seismic performance of outrigger braced system based on finite element and component-mode synthesis methods. Civil Engineering (Shiraz), 2020, 44(4): 1125−1133
44. Kamgar R, Rahgozar P. Optimum location for the belt truss system for minimum roof displacement of steel buildings subjected to critical excitation. Steel and Composite Structures, 2020, 37(4): 463−479
45. Kamgar R, Shojaee S, Rahgozar R. Rehabilitation of tall buildings by active control system subjected to critical seismic excitation. Asian Journal of Civil Engineering, 2015, 16(6): 819−833
46. Kamgar R, Mohammad R. Numerical study for evaluating the effect of length-to-height ratio on the behavior of concrete frame retrofitted with steel infill plates. Practice Periodical on Structural Design and Construction, 2022, 27(1): 04021062
47. Tavakoli R, Kamgar R, Rahgozar R. Optimal location of energy dissipation outrigger in high-rise building considering nonlinear soil-structure interaction effects. Periodica Polytechnica Civil Engineering, 2020, 64(3): 887−903
48. Kamgar R, Tavakoli R, Rahgozar P, Jankowski R. Application of discrete wavelet transform in seismic nonlinear analysis of soil-structure interaction problems. Earthquake Spectra, 2021, 37(3): 1980−2012
49. Zayas V A, Low S S, Mahin S A. A simple pendulum technique for achieving seismic isolation. Earthquake Spectra, 1990, 6(2): 317−333
50. Li Y, Lu X Z, Guan H, Ye L P. An energy-based assessment on dynamic amplification factor for linear static analysis in progressive collapse design of ductile RC frame structures. Advances in Structural Engineering, 2014, 17(8): 1217−1225
51. Jian H, Zheng Y. Simplified models of progressive collapse response and progressive collapse-resisting capacity curve of RC beam-column substructures. Journal of Performance of Constructed Facilities, 2014, 28(4): 04014008
52. Xu F J. Studies on displacement-based seismic design methodology of reinforced concrete frame-core wall structures. Dissertation for the Doctoral Degree. Beijing: Tsinghua University, 2006 (in Chinese)